

This document is confidential and is proprietary to the American Chemical Society and its authors. Do not copy or disclose without written permission. If you have received this item in error, notify the sender and delete all copies.

In-Cell Protein Structures from 2D NMR Experiments

Journal:	<i>The Journal of Physical Chemistry Letters</i>
Manuscript ID	jz-2016-01074z.R2
Manuscript Type:	Letter
Date Submitted by the Author:	01-Jul-2016
Complete List of Authors:	Müntener, Thomas; Universität Basel, Chemie Häussinger, Daniel; Universität Basel, Chemie Selenko, Philipp; Leibniz Institute of Molecular Pharmacology, Structural Biology Theillet, François-Xavier; CNRS, Institute of Integrative Biology of the Cell

SCHOLARONE™
Manuscripts

In-Cell Protein Structures from 2D NMR Experiments.

AUTHOR NAMES.

Thomas Müntener[†], Daniel Häussinger^{†}, Philipp Selenko[‡], Francois-Xavier Theillet^{*‡,§}*

[†]Department of Chemistry, University of Basel, St. Johannis-Ring 19, 4056 Basel, Switzerland,

[‡]Department of Structural Biology, Leibniz Institute of Molecular Pharmacology (FMP Berlin),
Robert Roessle Str. 10, 13125 Berlin, Germany

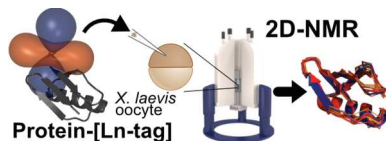
Corresponding Author

[*daniel.haeussinger@unibas.ch](mailto:daniel.haeussinger@unibas.ch)

[*francois-xavier.theillet@cnrs.fr](mailto:francois-xavier.theillet@cnrs.fr)

1
2
3 1 ABSTRACT.
4
5
6

7 2 In-cell NMR spectroscopy provides atomic resolution insights into the structural properties of
8
9
10 3 proteins in cells, but it is rarely used to solve entire protein structures *de novo*. Here, we
11
12 4 introduce a paramagnetic lanthanide-tag to simultaneously measure protein pseudocontact shifts
13
14 5 (PCSs) and residual dipolar couplings (RDCs) to be used as input for structure calculation
15
16 6 routines within the Rosetta program. We employ this approach to determine the structure of the
17
18 7 protein G B1 domain (GB1) in intact *Xenopus laevis* oocytes from a single set of 2D in-cell
19
20 8 NMR experiments. Specifically, we derive well-defined GB1 ensembles from low concentration
21
22 9 in-cell NMR samples ($\sim 50 \mu\text{M}$) measured at moderate magnetic field strengths (600 MHz), thus
23
24
25
26 10 offering an easily accessible alternative for determining intracellular protein structures.
27
28
29
30
31

32 12 TOC GRAPHICS
33
34
35

45 15 **KEYWORDS** Cellular structural biology, in-cell NMR, protein structure determination, NMR
46
47 16 spectroscopy, pseudocontact shifts, residual dipolar couplings.
48
49
50
51 17
52
53
54
55
56
57
58
59
60

1 Physical methods to delineate structural insights into the three-dimensional properties of
2 biomolecules such as X-ray crystallography, NMR spectroscopy or electron microscopy,
3 typically require experimental conditions and sample states that are vastly different from the
4 crowded intracellular environments in which these molecules natively occur¹. For these reasons,
5 considerable effort is put into the development of biophysical methods to directly study
6 biomolecules inside live cells. While high-resolution X-ray crystallography and single molecule
7 electron microscopy are inherently excluded from such *in vivo* experiments, due to the
8 requirement of crystalline or vitrified samples and the use of high-energy X-ray or electron
9 beams to generate experimental data, solution NMR spectroscopy can provide non-destructive
10 atomic-resolution information on individual biomolecules in cells. Specifically, in-cell NMR
11 spectroscopy^{2,3} takes advantage of the isotope-labeling effect to selectively ‘visualize’ isotope-
12 enriched, NMR-active proteins, RNA or DNA against the backdrop of all other non isotope-
13 labeled and NMR-inactive intracellular components. This enables direct NMR measurements
14 under truly physiological *in vivo* conditions. Following this rationale, in-cell NMR has been used
15 to derive insights into intracellular protein conformations,⁴ conformational equilibria,⁵ folding
16 and stability behaviors,⁶⁻⁸ protein dynamics,⁹ protein-protein and quinary protein interactions,^{9,10}
17 physiological redox states,¹¹ metal-binding properties¹² and post-translational protein
18 modifications.^{9,13,14} By contrast, the use of in-cell NMR to determine entire protein structures in
19 live cells is generally hampered by the limited lifetimes of in-cell NMR samples, their inherently
20 low concentrations of intracellular, isotope-enriched biomolecules (i.e. protein, RNA or DNA)
21 and their concomitantly poor spectral qualities. Especially lengthy 3D and 4D NMR experiments
22 - commonly used to derive long-range distance restraints for calculating biomolecular structures
23 - suffer from these drawbacks.¹⁵ Several advances in NMR methods, including faster acquisition

1 routines and non-uniform sampling procedures¹⁶⁻¹⁸ have helped to ameliorate some of these
2 shortcomings and enabled the first and only intracellular protein structure to be determined by in-
3 cell NMR spectroscopy in bacteria, although at exceedingly high, non-physiological intracellular
4 protein concentrations in the millimolar range⁴. As a result, and given the general poor sensitivity
5 of 3D and 4D NMR experiments even with such enhancing techniques, comprehensive structure
6 determination efforts of proteins in live cells are deemed impractical and unfeasible. Here, we
7 present an alternative approach to determine intracellular protein structures in live eukaryotic
8 cells that solely relies on 2D NMR experiments and paramagnetic protein tagging to
9 simultaneously induce pseudocontact shifts (PCSs) and residual dipolar couplings (RDCs). In
10 turn, we demonstrate how these structural parameters suffice to calculate high-precision in-cell
11 protein structures with the Rosetta program.

12 Tagging of proteins with different metals of the lanthanide series is known to induce strong
13 metal-specific distance- and orientation-dependent PCS effects on individual NMR-active atomic
14 nuclei.^{19,20} Such PCSs serve as powerful long-range distance restraints in structure calculation
15 routines and they can be derived from simple 2D NMR experiments, with different types of
16 lanthanide-binding protein tags (Fig. 1a).²¹⁻²⁴ Optimizing the rigidity and linker-lengths of
17 individual tag structures also enables partial alignments of coupled proteins with respect to the
18 external magnetic field, thus giving rise to measurable RDCs and, thereby, additional
19 orientational restraints (Fig. 1b).²⁵⁻²⁷ In a first step, we designed a modified version of the
20 classical tetraaza-carboxylic DOTA chelator, known for its excellent metal coordinating
21 properties, which we termed DOTA-M7Py (Fig. S1). This tag can be covalently coupled to the
22 sulfhydryl moiety of cysteine residues forming a non-reducible thioether bond.²⁸⁻³⁰ With regard
23 to in-cell PCS and RDC measurements, DOTA-M7Py displays several attractive features. First,

1
2
3 1 it is inherently rigid and adopts exclusively the square anti-prismatic $\Lambda(\delta\delta\delta\delta)$ stereo-confi-
4
5
6 2 guration for the *4S,3R*-Lu derivative.³¹ Second, it is neutral after binding to lanthanide metals.
7
8 3 Third, its linker portion is short, which reduces tag mobility and generates larger PCS effects,
9
10 4 thus providing higher precision structural information. Fourth, it features both hydrophilic and
11
12 5 hydrophobic properties (Fig. S1), which augment stable positioning on most protein surfaces,
13
14
15 6 further enhancing PCSs. Fifth, its thioether bond is expected to withstand the reducing
16
17 7 environment of the cytoplasm while maintaining DOTA's outstanding affinity towards
18
19 8 lanthanide metals ($K_d < 10^{-25}$ M).²⁷

20
21
22 9 We initially prepared diamagnetic DOTA-M7Py[Lu], and paramagnetic DOTA-M7Py[Tm]
23
24 10 and DOTA-M7Py[Tb] complexes, which we coupled to the Streptococcal protein G B1 domain
25
26 11 (GB1) via cysteine residues that we introduced by site-directed mutagenesis at individual GB1
27
28 12 positions, i.e., E19C, K28C and E42C. Using purified GB1 samples we recorded 2D ^1H - ^{15}N
29
30 13 HSQC spectra at 600 MHz, which revealed the expected PCS effects for the paramagnetic
31
32 14 species (up to 6 p.p.m., Fig. 1a; Fig. S2 & S3; Table S1). We also detected strong cross-peak
33
34 15 splitting in 2D ^1H - ^{15}N IPAP-HSQC spectra due to paramagnetic alignment of the GB1 domain
35
36 16 and resulting RDC effects³² (amplitudes reaching 25 Hz at 293 K, 600 MHz, Fig. 1b; Fig. S2 &
37
38 17 S4; Table S2). In agreement with the temperature dependency of the tag's mobility, we obtained
39
40 18 30 % higher or lower PCS and RDC values at 277 K and 310 K, respectively (Table S1 & S2).
41
42 19 Moreover, NMR spectra of the different DOTA-M7Py[Tm]-tagged GB1 samples (E19C, K28C
43
44 20 and E42C) revealed both positive and negative PCSs, as well as larger overall RDCs,^{19,20} which
45
46 21 is particularly useful for structure calculation routines. Therefore, we resorted to using DOTA-
47
48 22 M7Py[Tm]-GB1 samples in all further experiments.
49
50
51
52
53
54
55
56
57
58
59
60

1 Next, we microinjected tagged GB1 carrying either diamagnetic (Lu) or paramagnetic metals
2 (Tm) into *Xenopus laevis* oocytes for in-cell NMR measurements.^{3,33,34} We recorded 2D ¹H-¹⁵N
3 HSQC spectra at effective NMR concentrations of ~25 μM (intracellular GB1 concentrations
4 ~50 μM), which revealed PCSs that were virtually indistinguishable from the respective *in vitro*
5 samples with an overall RMSD of 0.04 p.p.m., corresponding to 24 and 2.4 Hz in the ¹H and ¹⁵N
6 dimensions, respectively (Fig. 1e; Fig. S2, S5 & S6). We did not detect sample degradation or
7 metal leakage for up to 24 hours, thus indicating the excellent stability of metal-loaded DOTA-
8 M7Py in *Xenopus* oocytes. Similarly, we measured in-cell RDCs that were comparable to those
9 obtained *in vitro* (Fig. 1d-1e, Fig. S7, Table S1 & S2). Because intracellular viscosity leads to
10 faster T2 relaxation and, accordingly, enhanced ¹⁵N signal decays, we chose to record in-cell
11 RDC experiments with the ¹⁵N free-induction decay (FID) set to 36 Hz, as opposed to 17 Hz for
12 RDC measurements *in vitro* (cf Material and Methods). This resulted in average GB1 ¹⁵N line
13 widths of ~30 Hz, compared to ~12 Hz *in vitro*, which, concomitantly, increased the RMSD of
14 RDCs measured *in vitro* versus in cells by 5 Hz, explaining also the larger differences of PCS
15 and RDC RMSDs.

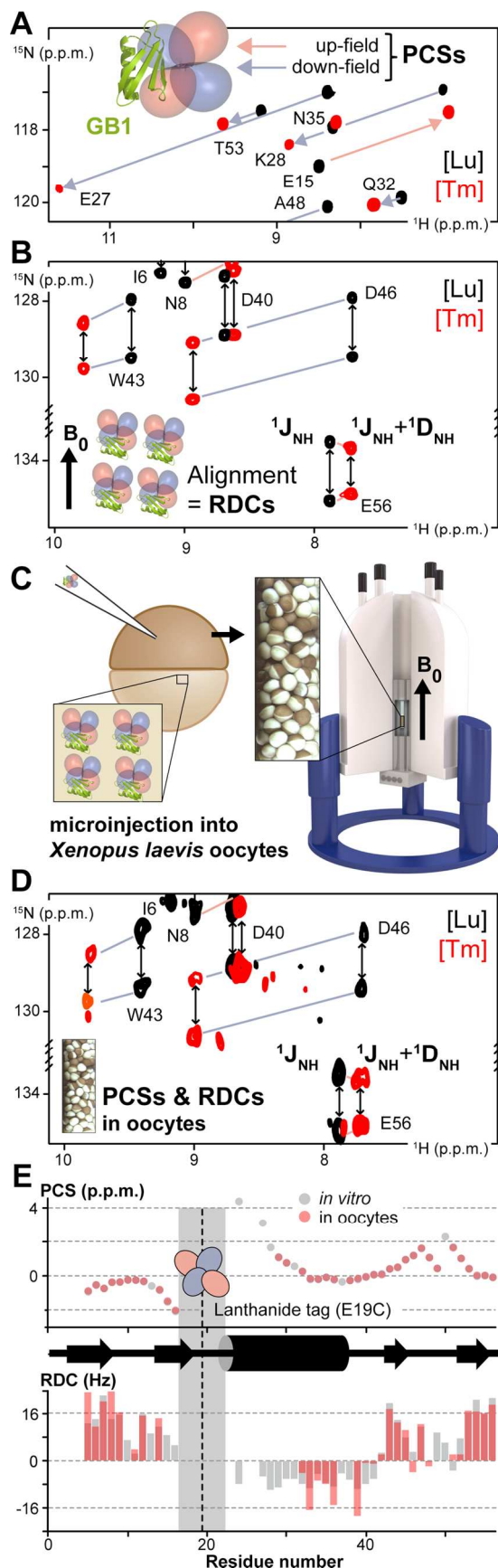


Figure 1. (A) Superposition of ^1H - ^{15}N 2D NMR spectra of purified GB1(E19C) coupled to DOTA-M7Py carrying diamagnetic Lutetium (Lu, black) or paramagnetic Thulium (Tm, red). Pseudocontact shift (PCS)-induced up- and down-field chemical shift changes are indicated (subset view). The inset depicts the GB1(E19C) ribbon structure (green) with paramagnetic iso-surfaces drawn at 2 p.p.m. (blue & red) (B) Superposition of 2D IPAP-HSQC spectra of GB1 with peak splitting due to amide scalar- ($^1J_{\text{NH}}$) and residual dipolar-coupling (RDC, i.e. $^1D_{\text{NH}}$). Paramagnetic GB1 alignment with respect to the external magnetic field (B_0) is shown schematically. (C) Overview of GB1 sample preparation in *Xenopus laevis* oocytes and (D) superposition of GB1 NMR spectra displaying in-cell PCS and RDC effects (at 600 MHz). (E) Residue-resolved quantification of *in vitro* & in-cell PCS and RDC data at 293 K and 600 MHz.

1
2
3
4 1 Finally, we used in-cell PCS and RDC data as input for GPS-Rosetta, a program that integrates
5
6 2 PCSs from multiple paramagnetic centers into unified distance constraints in structure
7
8 3 calculation routines.²³ Following the fragment-based rationale used by Rosetta, we generated
9
10 4 input libraries of 3- and 9-residue fragments of known protein structures, excluding the structure
11
12 5 of GB1 and homologous folds. Using these fragments, we generated 10,000 GB1 structures, out
13
14 6 of which we collected the 100 lowest-energy models and compared their conformations to
15
16 7 experimentally determined GB1 structures, i.e. X-ray crystallography (PDB code: 2QMT³⁵) and
17
18 8 solution NMR (PDB code: 1GB1³⁶, 2PLP³⁷). We found poor convergence of individual models,
19
20 9 with a median backbone C α RMSD of 1.85 Å (Fig. 2a). Next, we added a PCS-based ‘weight-
21
22 10 ing’ function to steer GB1 models towards conformations that recapitulated the measured values.
23
24
25 11 We used 72, 86 and 96 PCS constraints from the E19C, K28C and E42C GB1 mutants,
26
27 12 respectively, and obtained a substantially improved convergence of GB1 structures. The newly
28
29 13 determined average C α RMSD of the 100 lowest-energy models was 0.98 Å, and 0.64 Å
30
31 14 between the closest model and the crystal structure (Fig. 2b). Lastly, we used the RDC module of
32
33 15 Rosetta to include measured RDCs as additional input in our structure calculation routines,
34
35 16 which yielded a similar improved convergence of GB1 models (average C α RMSD of 1.04 Å for
36
37 17 the 100 lowest-energy structures, 0.64 Å for the closest model and the X-ray structure) (Fig. 2c).

38
39 18 Upon closer inspection of the 10 lowest energy structures, we noticed a remarkable difference
40
41 19 between structures obtained with PCS data alone and the ones for which PCS and RDC values
42
43 20 were used. In both ensembles, loop L1 (residues N8 to E15) connecting strands β 1 and β 2 of
44
45 21 GB1 displayed two distinct conformations. One identical to the X-ray structure with an average
46
47 22 C α RMSD of 1.1 Å, and one with a larger C α -deviation and average RMSD of 1.6 Å. In PCS
48
49 23 models, only three out of ten structures adopted the X-ray L1 conformation. In PCS+RDC
50
51
52
53
54
55
56
57
58
59
60

1 models, five out of ten structures did. Previous solution NMR data indicated that L1 is highly
 2 flexible with backbone order parameters (S^2) in the range of 0.5-0.6 (S^2 of GB1 regions with
 3 secondary structure ~ 0.8).³⁷⁻⁴⁰ These *in vitro* solution conformations of L1 are similar to those
 4 observed in GB1 crystals with an L1 C α RMSD of 1.35 Å (Fig. 2D). From this we concluded
 5 that combined PCS and RDC data from single 2D in-cell NMR experiments are sufficient to
 6 determine well-defined protein structures within PCS Rosetta. Our results further confirmed that
 7 the overall structural features of GB1 in *Xenopus* oocytes are similar to those observed *in vitro*.³⁴
 8

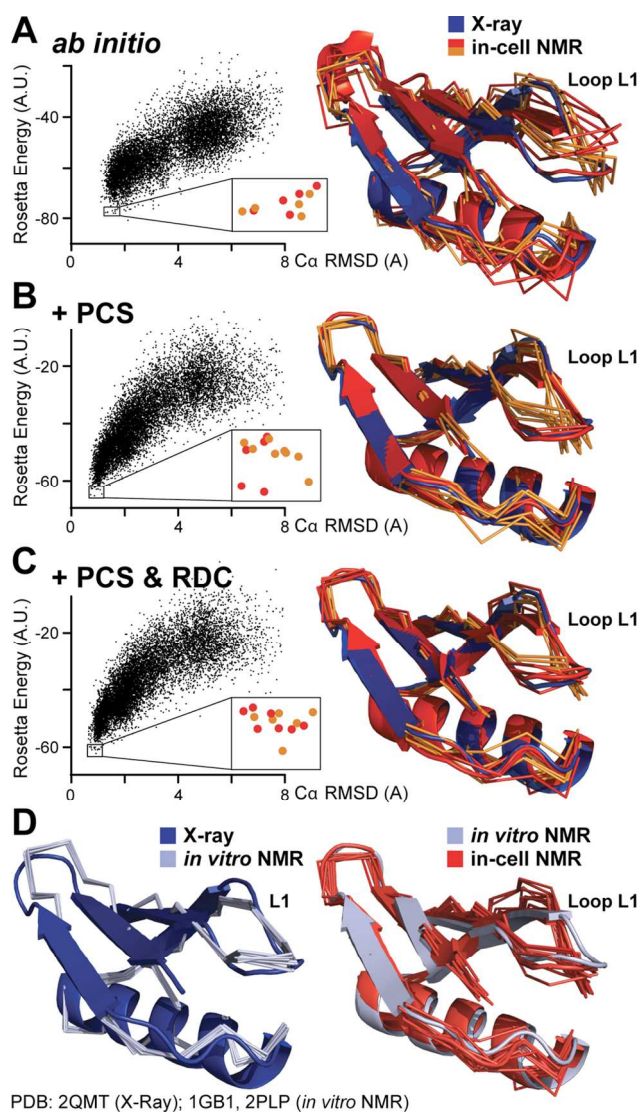


Figure 2. *In vitro* and in-cell structures of GB1. Scatter plots depict Rosetta energy scores and C α RMSDs of 10,000 GB1 models compared to the GB1 X-ray structure (2QMT). 10 lowest-energy structures are magnified and color-coded according their loop L1 conformations (red/orange). A superposition of their structures with the crystal conformation (blue) is shown on the right. GB1 models with L1 conformations corresponding to the one of the GB1 crystal are shown in red, deviating L1 conformers are colored orange. (A) *Ab initio* GB1 models without using experimental restraints, (B) GB1 models calculated with PCS and (C)

1 PCS+RDC input data. Rosetta energies contain different energy components and are not
2 comparable. (D) Left: Superposition of high-resolution *in vitro* solution NMR structures of
3 isolated GB1, i.e. 2PLP³⁷ (dark blue, ribbon representation) and 1GB1³⁶ (light blue, ensemble
4 representation). Right: Superposition of 2PLP (blue) and 10 lowest-energy in-cell GB1 models
5 (PCS+RDC, red).

6 In summary, we show that in-cell NMR-derived PCS and RDC data suffice to solve a protein's
7 structure inside cells. Whereas PCS effects decrease with the distance to the coordinated metal,
8 RDCs are distance-independent and offer valuable structural information for residues distal to
9 the paramagnetic center. PCS and RDC data can jointly be obtained from single 2D NMR
10 experiments on in-cell NMR samples of low intracellular protein concentrations, measured at
11 moderate magnetic field strengths, which makes them easily accessible and highly useful. The
12 presented approach can further be used for determining glycan and nucleic acid structures,^{2,41} as
13 well as to probe ligand interactions.⁴² In addition, the high rigidity of the DOTA-M7Py tag
14 renders it a useful tool for in-cell EPR studies.^{43,44} Given that the intracellular delivery of
15 paramagnetically tagged proteins into cultured mammalian cells by electroporation is
16 straightforward,⁹ combined PCS and RDC measurements in live cells also hold great promise for
17 future structure determination efforts in intact mammalian specimens.

18

19 **Supporting Information.**

20 The Supporting Information is available free of charge on the ACS Publications website. It
21 contains Material and Methods, Supporting Figures and Tables, in pdf format.

22 **Present Addresses**

1 § Department of Structural Biology, Institute of Integrative Biology of the Cell (I2BC) – UMR
2 9198, CNRS/CEA/Paris-Saclay University, CEA Saclay Bât. 144, 91191 Gif-sur-Yvette, France.

3 **Funding Sources**

4 This work was supported by the Agence Nationale pour la Recherche, grant ANR-14-ACHN-
5 0015-01 (FXT) and the Fondation Claude et Giuliana, Vaduz, Liechtenstein (TM). PS is
6 supported by an ERC Consolidator Grant #647474 NeuroInCellNMR.

7 **Notes**

8 Any additional relevant notes should be placed here.
9 The authors declare no competing financial interests.

10 **Acknowledgement**

11 We thank M. van Rossum for laboratory management, and H. Naumann for her kind
12 hospitality. Calculations were performed at the sciCORE scientific computing core facility
13 (<http://scicore.unibas.ch/>) at the University of Basel. Support by M.Jacquot and K. Arnold is
14 gratefully acknowledged. We thank C.E. Housecroft and E.C. Constable for helpful discussions
15 and R.A. Byrd for providing chemicals.

17 **References**

18 (1) Theillet, F.-X.; Binolfi, A.; Frembgen-Kesner, T.; Hingorani, K.; Sarkar, M.; Kyne, C.;
19 Li, C.; Crowley, P. B.; Gierasch, L.; Pielak, G. J.; *et al.* Physicochemical Properties of Cells and
20 Their Effects on Intrinsically Disordered Proteins (IDPs). *Chem. Rev.* **2014**, *114*, 6661–6714.

- 1
2
3
4 1 (2) Hänsel, R.; Luh, L. M.; Corbeski, I.; Trantirek, L.; Dötsch, V. In-Cell NMR and EPR
5
6 2 Spectroscopy of Biomacromolecules. *Angew. Chem. Int. Ed.* **2014**, *53*, 10300–10314.
7
8
9 3 (3) Freedberg, D. I.; Selenko, P. Live Cell NMR. *Annu. Rev. Biophys.* **2014**, *43*, 171–192.
10
11
12 4 (4) Sakakibara, D.; Sasaki, A.; Ikeya, T.; Hamatsu, J.; Hanashima, T.; Mishima, M.;
13
14 5 Yoshimasu, M.; Hayashi, N.; Mikawa, T.; Wälchli, M.; et al. Protein Structure Determination in
15
16 6 Living Cells by in-Cell NMR Spectroscopy. *Nature* **2009**, *458*, 102–105.
17
18
19
20 7 (5) Ye, Y.; Liu, X.; Xu, G.; Liu, M.; Li, C. Direct Observation of Ca²⁺-Induced Calmodulin
21
22 8 Conformational Transitions in Intact *Xenopus Laevis* Oocytes by ¹⁹F NMR Spectroscopy.
23
24 9 *Angew. Chem. Int. Ed.* **2015**, *127*, 5418–5420.
25
26
27
28 10 (6) Monteith, W. B.; Cohen, R. D.; Smith, A. E.; Guzman-Cisneros, E.; Pielak, G. J. Quinary
29
30 11 Structure Modulates Protein Stability in Cells. *Proc. Natl. Acad. Sci. USA* **2015**, *112*, 1739–
31
32 12 1742.
33
34
35
36 13 (7) Danielsson, J.; Mu, X.; Lang, L.; Wang, H.; Binolfi, A.; Theillet, F.-X.; Bekei, B.; Logan,
37
38 14 D. T.; Selenko, P.; Wennerstrom, H.; et al. Thermodynamics of Protein Destabilization in Live
39
40 15 Cells. *Proc. Natl. Acad. Sci. U.S.A.* **2015**, *112*, 12402–12407.
41
42
43
44 16 (8) Luchinat, E.; Barbieri, L.; Rubino, J. T.; Kozyreva, T.; Cantini, F.; Banci, L. In-Cell
45
46 17 NMR Reveals Potential Precursor of Toxic Species From SOD1 fALS Mutants. *Nat. Commun.*
47
48 18 **2014**, *5*, 5502.
49
50
51
52 19 (9) Theillet, F.-X.; Binolfi, A.; Bekei, B.; Martorana, A.; Rose, H. M.; Stuver, M.; Verzini,
53
54 20 S.; Lorenz, D.; van Rossum, M.; Goldfarb, D.; et al. Structural Disorder of Monomeric A-
55
56 21 Synuclein Persists in Mammalian Cells. *Nature* **2016**, *530*, 1–19.
57
58
59
60

- 1
2
3 1 (10) Majumder, S.; Xue, J.; DeMott, C. M.; Reverdatto, S.; Burz, D. S.; Shekhtman, A.
4
5 2 Probing Protein Quinary Interactions by in-Cell Nuclear Magnetic Resonance Spectroscopy.
6
7
8 3 *Biochemistry* **2015**, *54*, 2727–2738.
9
10
11 4 (11) Barbieri, L.; Bertini, I.; Luchinat, E.; Secci, E.; Zhao, Y.; Banci, L.; Aricescu, A. R.
12
13 5 Atomic-Resolution Monitoring of Protein Maturation in Live Human Cells by NMR. *Nat. Chem.*
14
15 6 *Biol.* **2013**, *9*, 297–299.
16
17
18 7 (12) Banci, L.; Barbieri, L.; Bertini, I.; Cantini, F.; Luchinat, E. In-Cell NMR in *E. Coli* to
19
20 8 Monitor Maturation Steps of hSOD1. *PLoS ONE* **2011**, *6*, 1–8.
21
22
23 9 (13) Selenko, P.; Frueh, D. P.; Elsaesser, S. J.; Haas, W.; Gygi, S. P.; Wagner, G. In Situ
24
25 10 Observation of Protein Phosphorylation by High-Resolution NMR Spectroscopy. *Nat. Struct.*
26
27 11 *Mol. Biol.* **2008**, *15*, 321–329.
28
29
30
31
32 12 (14) Binolfi, A.; Limatola, A.; Verzini, S.; Kosten, J.; Theillet, F.-X.; May Rose, H.; Bekei,
33
34 13 B.; Stuiver, M.; van Rossum, M.; Selenko, P. Intracellular Repair of Oxidation-Damaged A-
35
36 14 Synuclein Fails to Target C-Terminal Modification Sites. *Nat. Commun.* **2016**, *7*, 10251.
37
38
39
40 15 (15) Rosato, A.; Vranken, W.; Fogh, R. H.; Ragan, T. J.; Tejero, R.; Pederson, K.; Lee, H.-W.;
41
42 16 Prestegard, J. H.; Yee, A.; Bin Wu; *et al.* The Second Round of Critical Assessment of
43
44 17 Automated Structure Determination of Proteins by NMR: CASD-NMR-2013. *J. Biomol. NMR*
45
46 18 **2015**, *62*, 413–424.
47
48
49
50 19 (16) Waudby, C. A.; Christodoulou, J. An Analysis of NMR Sensitivity Enhancements
51
52 20 Obtained Using Non-Uniform Weighted Sampling, and the Application to Protein NMR. *J.*
53
54 21 *Magn. Reson.* **2012**, *219*, 46–52.
55
56
57
58
59
60

- 1
2
3 1 (17) Hyberts, S. G.; Robson, S. A.; Wagner, G. Exploring Signal-to-Noise Ratio and
4
5 2 Sensitivity in Non-Uniformly Sampled Multi-Dimensional NMR Spectra. *J. Biomol. NMR* **2012**,
6
7 3 55, 167–178.
8
9
10
11 4 (18) Palmer, M. R.; Suiter, C. L.; Henry, G. E.; Rovnyak, J.; Hoch, J. C.; Polenova, T.;
12
13 5 Rovnyak, D. Sensitivity of Nonuniform Sampling NMR. *J. Phys. Chem. B* **2015**, *119*, 6502–
14
15 6 6515.
16
17
18
19 7 (19) Otting, G. Protein NMR Using Paramagnetic Ions. *Annu. Rev. Biophys.* **2010**, *39*, 387–
20
21 8 405.
22
23
24
25 9 (20) Koehler, J.; Meiler, J. Expanding the Utility of NMR Restraints with Paramagnetic
26
27 10 Compounds: Background and Practical Aspects. *Prog. Nucl. Magn. Reson. Spectrosc.* **2011**, *59*,
28
29 11 360–389.
30
31
32
33 12 (21) Schmitz, C.; Vernon, R.; Otting, G.; Baker, D.; Huber, T. Protein Structure
34
35 13 Determination From Pseudocontact Shifts Using ROSETTA. *J. Mol. Biol.* **2012**, *416*, 668–677.
36
37
38
39 14 (22) Rinaldelli, M.; Ravera, E.; Calderone, V.; Parigi, G.; Murshudov, G. N.; Luchinat, C.
40
41 15 Simultaneous Use of Solution NMR and X-Ray Data in REFMAC5 for Joint
42
43 16 Refinement/Detection of Structural Differences. *Acta Crystallogr. D Biol. Crystallogr.* **2014**, *70*,
44
45 17 958–967.
46
47
48
49 18 (23) Yagi, H.; Pilla, K. B.; Maleckis, A.; Graham, B.; Huber, T.; Otting, G. Three-
50
51 19 Dimensional Protein Fold Determination From Backbone Amide Pseudocontact Shifts Generated
52
53 20 by Lanthanide Tags at Multiple Sites. *Structure* **2013**, *21*, 883–890.
54
55
56
57
58
59
60

- 1
2
3 1 (24) Brewer, K. D.; Bacaj, T.; Cavalli, A.; Camilloni, C.; Swarbrick, J. D.; Liu, J.; Zhou, A.;
4
5 2 Zhou, P.; Barlow, N.; Xu, J.; *et al.* Dynamic Binding Mode of a Synaptotagmin-1-SNARE
6
7 3 Complex in Solution. *Nat. Struct. Mol. Biol.* **2015**, *22*, 555–564.
8
9
10
11 4 (25) Salmon, L.; Blackledge, M. Investigating Protein Conformational Energy Landscapes
12
13 5 and Atomic Resolution Dynamics From NMR Dipolar Couplings: a Review. *Rep Prog Phys*
14
15 6 **2015**, *78*, 126601.
16
17
18
19 7 (26) Su, X.-C.; McAndrew, K.; Huber, T.; Otting, G. Lanthanide-Binding Peptides for NMR
20
21 8 Measurements of Residual Dipolar Couplings and Paramagnetic Effects From Multiple Angles.
22
23 9 *J. Am. Chem. Soc.* **2008**, *130*, 1681–1687.
24
25
26
27 10 (27) Häussinger, D.; Huang, J.-R.; Grzesiek, S. DOTA-M8: an Extremely Rigid, High-
28
29 11 Affinity Lanthanide Chelating Tag for PCS NMR Spectroscopy. *J. Am. Chem. Soc.* **2009**, *131*,
30
31 12 14761–14767.
32
33
34
35 13 (28) Liu, W.-M.; Skinner, S. P.; Timmer, M.; Blok, A.; Hass, M. A. S.; Filippov, D. V.;
36
37 14 Overhand, M.; Ubbink, M. A Two-Armed Lanthanoid-Chelating Paramagnetic NMR Probe
38
39 15 Linked to Proteins via Thioether Linkages. *Chem. Eur. J.* **2014**, *20*, 6256–6258.
40
41
42
43 16 (29) Toda, N.; Asano, S.; Barbas, C. F. Rapid, Stable, Chemoselective Labeling of Thiols with
44
45 17 Julia-Kocięński-Like Reagents: a Serum-Stable Alternative to Maleimide-Based Protein
46
47 18 Conjugation. *Angew. Chem. Int. Ed.* **2013**, *52*, 12592–12596.
48
49
50
51 19 (30) Yang, Y.; Wang, J.-T.; Pei, Y.-Y.; Su, X.-C. Site-Specific Tagging Proteins via a Rigid,
52
53 20 Stable and Short Thiolether Tether for Paramagnetic Spectroscopic Analysis. *Chem. Commun.*
54
55 21 **2015**, *51*, 2824–2827.
56
57
58
59
60

- 1
2
3
4 1 (31) Opina, A. C. L.; Strickland, M.; Lee, Y.-S.; Tjandra, N.; Andrew Byrd, R.; Swenson, R.
5
6 2 E.; Vasalatiy, O. Analysis of the Isomer Ratios of Polymethylated-DOTA Complexes and the
7
8 3 Implications on Protein Structural Studies. *Dalton Trans.* **2016**, *4*, 4673–4687.
9
10
11 4 (32) Ottiger, M.; Delaglio, F.; Bax, A. Measurement of J and Dipolar Couplings From
12
13 5 Simplified Two-Dimensional NMR Spectra. *J. Magn. Reson.* **1998**, *131*, 373–378.
14
15
16
17 6 (33) Hänsel, R.; Luh, L. M.; Corbeski, I.; Trantirek, L.; Dötsch, V. In-Cell NMR and EPR
18
19 7 Spectroscopy of Biomacromolecules. *Angew. Chem. Int. Ed.* **2014**, *53*, 10300–10314.
20
21
22
23 8 (34) Selenko, P.; Serber, Z.; Gadea, B.; Ruderman, J.; Wagner, G. Quantitative NMR Analysis
24
25 9 of the Protein G B1 Domain in *Xenopus Laevis* Egg Extracts and Intact Oocytes. *Proc. Natl.*
26
27 10 *Acad. Sci. USA* **2006**, *103*, 11904–11909.
28
29
30
31 11 (35) Schmidt, H. L. F.; Sperling, L. J.; Gao, Y. G.; Wylie, B. J.; Boettcher, J. M.; Wilson, S.
32
33 12 R.; Rienstra, C. M. Crystal Polymorphism of Protein GB1 Examined by Solid-State NMR
34
35 13 Spectroscopy and X-Ray Diffraction. *J. Phys. Chem. B* **2007**, *111*, 14362–14369.
36
37
38
39 14 (36) Gronenborn, A. M.; Filpula, D. R.; Essig, N. Z.; Achari, A.; Whitlow, M.; Wingfield, P.
40
41 15 T.; Clore, G. M. A Novel, Highly Stable Fold of the Immunoglobulin Binding Domain of
42
43 16 Streptococcal Protein G. *Nature* **1991**, *253*, 657–661.
44
45
46
47 17 (37) Bouvignies, G.; Meier, S.; Grzesiek, S.; Blackledge, M. Ultrahigh-Resolution Backbone
48
49 18 Structure of Perdeuterated Protein GB1 Using Residual Dipolar Couplings From Two Alignment
50
51 19 Media. *Angew. Chem. Int. Ed.* **2006**, *45*, 8166–8169.
52
53
54
55
56
57
58
59
60

- 1
2
3 1 (38) Shapiro, Y. E.; Meirovitch, E. Slowly Relaxing Local Structure (SRLS) Analysis of ^{15}N -
4 H Relaxation From the Prototypical Small Proteins GB1 and GB3. *J. Phys. Chem. B* **2012**, *116*,
5 4056–4068.
6
7
8
9
10
11 4 (39) Lamley, J. M.; Lougher, M. J.; Sass, H. J.; Rogowski, M.; Grzesiek, S.; Lewandowski, J.
12 R. Unraveling the Complexity of Protein Backbone Dynamics with Combined (^{13}C) and (^{15}N)
13 Solid-State NMR Relaxation Measurements. *Phys. Chem. Chem. Phys.* **2015**, *17*, 21997–22008.
14
15
16
17
18
19 7 (40) Vögeli, B.; Kazemi, S.; Güntert, P.; Riek, R. Spatial Elucidation of Motion in Proteins by
20 Ensemble-Based Structure Calculation Using Exact NOEs. *Nat. Struct. Mol. Biol.* **2012**, *19*,
21 1053–1057.
22
23
24
25
26
27 10 (41) Canales, Á.; Mallagaray, Á.; Berbís, M. Á.; Navarro-Vázquez, A.; Domínguez, G.;
28 Cañada, F. J.; André, S.; Gabius, H.-J.; Pérez-Castells, J.; Jiménez-Barbero, J. Lanthanide-
29 Chelating Carbohydrate Conjugates Are Useful Tools to Characterize Carbohydrate
30 Conformation in Solution and Sensitive Sensors to Detect Carbohydrate–Protein Interactions. *J.*
31 *Am. Chem. Soc.* **2014**, *136*, 8011–8017.
32
33
34
35
36
37
38
39
40 15 (42) Guan, J.-Y.; Keizers, P. H. J.; Liu, W.-M.; Lohr, F.; Skinner, S. P.; Heeneman, E. A.;
41 Schwalbe, H.; Ubbink, M.; Siegal, G. Small-Molecule Binding Sites on Proteins Established by
42 Paramagnetic NMR Spectroscopy. *J. Am. Chem. Soc.* **2013**, *135*, 5859–5868.
43
44
45
46
47
48 18 (43) Martorana, A.; Bellapadrona, G.; Feintuch, A.; Di Gregorio, E.; Aime, S.; Goldfarb, D.
49 Probing Protein Conformation in Cells by EPR Distance Measurements Using Gd^{3+} Spin
50 Labeling. *J. Am. Chem. Soc.* **2014**, *136*, 13458–13465.
51
52
53
54
55
56
57
58
59
60

- 1
2
3 (44) Bleicken, S.; Jeschke, G.; Stegmüller, C.; Salvador-Gallego, R.; García-Sáez, A. J.;
4
5
6 2 Bordignon, E. Structural Model of Active Bax at the Membrane. *Molecular Cell* **2014**, *56*, 496–
7
8 3 505.
9
10
11 4
12
13
14
15
16
17
18
19
20
21
22
23
24
25
26
27
28
29
30
31
32
33
34
35
36
37
38
39
40
41
42
43
44
45
46
47
48
49
50
51
52
53
54
55
56
57
58
59
60